# PCCP



View Article Online **PAPER** 



Cite this: Phys. Chem. Chem. Phys., 2022, 24, 18552

# Confirmation of gaseous methanediol from stateof-the-art theoretical rovibrational characterization†

Megan C. Davis, Noah R. Garrett and Ryan C. Fortenberry \*\*D\*\*

High-level rovibrational characterization of methanediol, the simplest geminal diol, using state-of-theart, purely ab initio techniques unequivocally confirms previously reported gas phase preparation of this simplest geminal diol in its  $C_2$  conformation. The F12-TZ-cCR and F12-DZ-cCR quartic force fields (QFFs) utilized in this work are among the largest coupled cluster-based anharmonic frequencies computed to date, and they match the experimental band origins of the spectral features in the 980-1100 cm<sup>-1</sup> range to within 3 cm<sup>-1</sup>, representing a significant improvement over previous studies. The simulated spectrum also matches the experimental spectrum in the strong Q branch feature and qualitative shape of the 980–1100 cm<sup>-1</sup> region. Additionally, the full set of rotational constants, anharmonic vibrational frequencies, and quartic and sextic distortion constants are provided for both the lowest energy  $C_2$  conformer as well as the slightly higher  $C_s$  conformer. Several vibrational modes have intensities of 60 km mol<sup>-1</sup> or higher, facilitating potential astronomical or atmospheric detection of methanediol or further identification in laboratory work especially now that gas phase synthesis of this molecule has been established

Received 7th May 2022, Accepted 21st July 2022

DOI: 10.1039/d2cp02076a

rsc.li/pccp

#### 1 Introduction

Methanediol (CH<sub>2</sub>(OH)<sub>2</sub>), the simplest geminal diol, is a key intermediate in aerosol chemistry.1,2 It has recently been identified as a key part of formic acid producing pathways, 3,4 which plays a part in acidification of rainwater<sup>5</sup> and in cloud nucleation.6 The interactions of stable geminal diols with byproducts of Criegee-intermediate formation are, subsequently, likely vital in atmospheric chemistry. 7,8 Astrochemically, methanediol is predicted to be formed on interstellar ice grains<sup>9-11</sup> and goes on to participate in the formation of complex organic molecules.

Despite this importance, methanediol has long been elusive to observe in the gas phase, although it had been experimentally characterized in aqueous solutions, 12-16 through computational modeling, 17-19 and in Ar matrix analysis. 20 Most notably, in 2021, Jian et al. experimentally characterized a portion of the infrared, gas phase spectrum of methanediol<sup>21</sup> through analysis of a mixture of formaldehyde and water vapour in the gas phase. The authors also performed computational analysis to assign features

Department of Chemistry & Biochemistry, University of Mississippi, University, MS, 38677-1848. USA. E-mail: r410@olemiss.edu

of the resulting spectra using the B3LYP hybrid functional 22,23 with an aug-cc-pVTZ basis set.24 They assign the O-C-O antisymmetric and symmetric stretches as the origin of the rovibrational feature in the range of 980-1100 cm<sup>-1</sup>, with experimental band origins at 1580 cm<sup>-1</sup> and 1027 cm<sup>-1</sup>, respectively.

Zhu et al. then reported successful synthesis and detection of gaseous methanediol in 2021.25 Gaseous methanediol is prepared by exposing methanol-oxygen ices to high energy electrons followed by sublimation. Analysis with photoionizationreflectron time-of-flight mass spectrometry subsequently identifies the species together with IR spectroscopy.

Following this, a method for rapid preparation of gaseous methanediol was reported earlier this year by Chen and Chu.<sup>26</sup> An aqueous formaldehyde solution is evaporated allowing for measurement of the IR absorption spectrum of the vapour. The rovibrational feature at 980–1100 cm<sup>-1</sup> is free from interference of water and formaldehyde, and is identified as methanediol using the computational data from Jian et al. from the experimental band origins and B3LYP/aug-cc-pVTZ rotational parameters. While such theoretical confirmation is common, higher-level methods are really needed in order to verify the spectral features beyond mere empirically-fitted density functional theory results.

The present work utilizes highly accurate ab initio QFFs to provide accurate spectroscopic data to comment upon the identification of the 980-1100 cm<sup>-1</sup> rovibrational feature. High

<sup>†</sup> Electronic supplementary information (ESI) available: Harmonic vibrational frequencies of C2 methanediol and data from this work for C5 methanediol. See DOI: https://doi.org/10.1039/d2cp02076a

**PCCP Paper** 

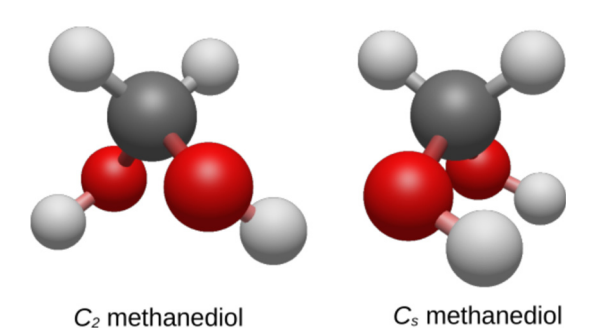


Fig. 1 Structures of methanediol conformers, where red atoms are oxygen, black are carbon and white are hydrogen.

level QFFs based on coupled cluster theory<sup>27–29</sup> produce anharmonic vibrational frequencies that are often within 5 cm<sup>-1</sup> of experiment and 30 MHz for rotational constants. 30-42 In this work the newly developed F12-TZ-cCR and F12-DZ-cCR QFFs, which produce exceptional accuracies of better even than 1 cm<sup>-1</sup> for vibrational frequencies in many cases, <sup>43</sup> are utilized to attain this high accuracy for modest computational cost. The spectroscopic data provided by this work will also aid in possible future detections of methanediol in laboratory synthesis or in the interstellar medium. With the advent of the new approach for synthesizing methanediol in the gas phase from Chen and Chu, these rovibrational spectral data are absolutely essential for complete rovibrational characterization of this molecule.

## 2 Computational methods

QFFs are utilized in this work in order to efficiently compute the anharmonic vibrational frequencies and other spectroscopic data for both the  $C_s$  and  $C_2$  conformations of methanediol (Fig. 1). The F12-TZ-cCR and F12-DZ-cCR approaches are utilized as the cheaper and more accurate alternative than other more costly composite QFF methods. 43 These approaches are based on coupled cluster theory at the singles, doubles, and perturbative triples [CCSD(T)] level of theory<sup>27–29</sup> with the explicitly correlated F12b formalism (CCSD(T)-F12b).44

First, the geometries for both conformations of methanediol are optimized. The cc-pCVTZ-F12 and cc-pCVDZ-F12 basis sets along with the CCSD(T)-F12b method are employed including core electron correlation for the F12-TZ-cCR and F12-DZ-cCR. Since the F12-DZ-cCR QFF only differs in basis set quality, the double zeta level is used to evaluate the accuracy of a cheaper method and to determine if the double zeta quality can produce accurate results for a lower computational cost. After the optimized geometries are obtained for both conformations, single-point CCSD(T)-F12b energies including core electrons and an additional CCSD(T) Douglas-Kroll scalar relativistic correction<sup>46</sup> are computed for a set of displacements using symmetry internal coordinates. The symmetry internal coordinates for the  $C_s$  confirmation of  $CH_2OH_2$  are given in eqn (1)-(15), requiring 19585 total displacements.  $C_2$  methanediol coordinates are given in eqn (16)-(30) and require slightly

fewer, specifically 19525 total, displacements to construct the QFF. The H<sub>1</sub> and H<sub>2</sub> atoms are attached to the central carbon atom, and H<sub>3</sub> is attached to O<sub>1</sub> with H<sub>4</sub> attached to O<sub>2</sub>. These represent some of the largest coupled cluster-based QFFs computed to date. Additionally, they contain three heavy atoms making them among the most computationally-intensive, large QFFs computed thus far.

Following computation of the single point energies, a leastsquares fit is performed to generate force constants, followed by a refit to zero the gradients. INTDER2005<sup>47</sup> then transforms the force constants from symmetry-internal to Cartesian coordinates. SPECTRO,48 which uses second-order rotational and vibrational perturbation theory (VPT2), 49-51 is then used in order to calculate the rovibrational spectral data for both conformations of methanediol, Fermi, Coriolis, and Darling-Dennison resonances included in the VPT2 calculations are given in Table S1 (ESI†). Considerations of nuclear spin are left for future work as these would require additional computations beyond the QFFs generated here.

The Molpro quantum chemistry software<sup>45</sup> is used in most cases save for MP2/aug-cc-pVTZ anharmonic intensities from GAUSSIAN16.52 From these data, theoretical spectra is generated with PGOPHER,<sup>53</sup> using a Gaussian value of 0.45 cm<sup>-1</sup> for the line widths and using relative anharmonic intensities and other spectral data calculated herein. The simulation is performed at 298 K similar to the experimental conditions of Chen and Chu.26

$$S_1(a') = H_1 - C \tag{1}$$

$$S_2(a') = \mathbf{H}_2 - \mathbf{C} \tag{2}$$

$$S_3(a') = (O_1 - C) + (O_2 - C)$$
 (3)

$$S_4(a') = (O_1 - H_3) + (O_2 - H_4)$$
 (4)

$$S_5(a') = \angle (H_1 - C - H_2) \tag{5}$$

$$S_6(a') = \angle (O_1 - C - H_1) + \angle (O_2 - C - H_1)$$
 (6)

$$S_7(a') = \angle (C - O_1 - H_3) + \angle (C - O_2 - H_4)$$
 (7)

$$S_8(a') = \tau(O_1 - C - H_1 - H_2) - \tau(O_2 - C - H_1 - H_2)$$
 (8)

$$S_9(a') = \tau(H_3 - O_1 - C - H_1) - \tau(H_4 - O_2 - C - H_2)$$
 (9)

$$S_{10}(a'') = (C-O_1) + (C-O_2)$$
 (10)

$$S_{11}(a'') = (O_1 - H_3) + (O_2 - H_4)$$
 (11)

$$S_{12}(a'') = \angle (O1-C-H_1) + \angle (O_2-C-H_1)$$
 (12)

$$S_{13}(a'') = \angle (C - O_1 - H_3) + \angle (C - O_2 - H_4)$$
 (13)

$$S_{14}(a'') = \tau(O_1 - C - H_1 - H_2) - \tau(O_2 - C - H_1 - H_2)$$
 (14)

$$S_{15}(a'') = \tau(H_3 - O_1 - C - H_1) - \tau(H_4 - O_2 - C - H_1)$$
 (15)

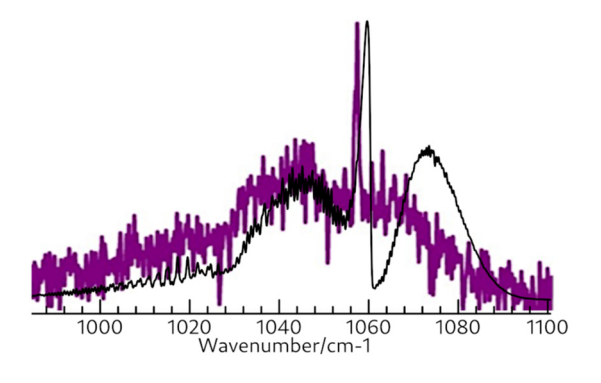
$$S_1(a) = (C-H_1) + (C-H_2)$$
 (16)

$$S_2(a) = (C-O_1) + (C-O_2)$$
 (17)

$$S_3(a) = (O_1 - H_3) + (O_2 - H_4)$$
 (18)

$$S_4(a) = \angle (H_1 - C - H_2)$$
 (19)

**PCCP** Paper



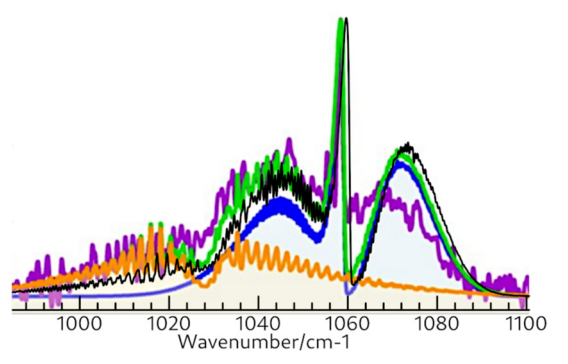


Fig. 2 Convolved F12-TZ-cCR spectra (black) from the corresponding  $\nu_{10}$ (blue) and  $\nu_{11}$  (orange) features overlaid with experimental spectra (purple) and B3LYP (green) from Chen and Chu.<sup>26</sup>

$$S_5(a) = \angle (O_1 - C - H_1) + \angle (O_2 - C - H_2)$$
 (20)

$$S_6(a) = \angle (C - O_1 - H_3) + \angle (C - O_2 - H_4)$$
 (21)

$$S_7(a) = \tau(O_1 - C - H_1 - H_2) + \tau(O_2 - C - H_2 - H_1)$$
 (22)

$$S_8(a) = \tau(H_3 - O_1 - C - H_1) + \tau(H_4 - O_2 - C - H_2)$$
 (23)

$$S_9(b) = (C-H_1) - (C-H_2)$$
 (24)

$$S_{10}(b) = (C-O_1) - (C-O_2)$$
 (25)

 $S_{11}(b) = (O_1 - H_3) - (O_2 - H_4)$ (26)

$$S_{12}(b) = \angle (O_1 - C - H_1) - \angle (O_2 - C - H_2)$$
 (27)

$$S_{13}(b) = \angle (C-O_1-H_3) - \angle (C-O_2-H_4)$$
 (28)

$$S_{14}(b) = \tau (O_1 - C - H_1 - H_2) - \tau (O_2 - C - H_2 - H_1)$$
 (29)

$$S_{15}(b) = \tau(H_3 - O_1 - C - H_1) - \tau(H_4 - O_2 - C - H_2)$$
 (30)

#### 3 Results and discussion

The simulated, pure ab initio F12-TZ-cCR spectra for the combined  $\nu_{10}$  and  $\nu_{11}$  C=O antisymmetric and symmetric stretches, respectively, (including the vibrationally-averaged rotational constants of both fundamentals) for the  $C_2$  conformation of methanediol is shown in Fig. 2. In the top portion, the black computed spectrum almost exactly matches the experimental IR data of Chen and Chu for this rovibrational feature in the 980-1100 cm<sup>-1</sup> range.<sup>26</sup> This provides unambiguous confirmation of Chen and Chu's successful preparation of methanediol in the gas-phase. The F12-TZ-cCR spectrum additionally matches with the authors' previous spectrum produced with experimental band origins and B3LYP/aug-cc-pVTZ rotational constants, also shown in green in the bottom of Fig. 2. The strong Q branch feature arising from the a-type  $\nu_{10}$  transition as well as the shoulder from approximately 980 cm<sup>-1</sup> to 1060 cm<sup>-1</sup>, consisting of both the P branch of  $\nu_{10}$  and the b-type  $\nu_{11}$  rovibrational feature, strongly support this feature arising from the presence of methanediol. The individual contributions from the  $\nu_{10}$  and  $\nu_{11}$  features to the overall spectrum can be seen in the blue and orange traces in the bottom of Fig. 2 as well as in Fig. S1 (ESI $\dagger$ ) Only the  $C_2$  conformation is considered in the spectral simulation, as the relative, anharmonic, zeropoint energy-corrected energy between the two conformers is calculated to be 781.28 cm<sup>-1</sup> at the F12-TZ-cCR level, resulting in a negligible Boltzmann ratio of 0.02 for  $C_s$  relative to  $C_2$  at

**Table 1**  $C_2$  Methanediol anharmonic vibrational frequencies in cm<sup>-1</sup>

		F12-XZ-cCR		Jian et al. <sup>21</sup>		Lugez et al. <sup>20 b</sup>	Barrient	Barrientos et al. 17	
Mode	Description	TZ	DZ	Int.a	B3LYP	Gas Phase	Argon Matrix	MP2	QCISD
$\overline{\nu_1(a)}$	sym. OH stret.	3647.6	3651.4	30	3617		3638.8-3637.6	3648	3711
$\nu_2(b)$	anti. OH stret.	3647.9	3651.7	50	3612		3564.4	3648	3710
$\nu_3(b)$	anti. CH stret.	2978.4	2978.6	33	2937		2977.7	3020	3007
$\nu_4(a)$	sym. CH stret.	2923.3	2929.3	31	2897			2807	2956
$\nu_5(a)$	CH <sub>2</sub> sciss.	1503.6	1505.4	1	1486			1374	1498
$\nu_6(b)$	CH <sub>2</sub> wag.	1404.5	1414.0	30	1413		1425.7-1424.4	1441	1413
$\nu_7(a)$	CH <sub>2</sub> twist	1351.4	1358.6	2	1354		1358.7-1353.8	1350	1360
$\nu_8(b)$	anti. COH bend	1334.2	1339.4	18	1311		1334.6	1329	1341
$\nu_9(a)$	sym. COH bend	1198.7	1196.5	2	1176			1188	1178
$\nu_{10}(b)$	anti. OCO stret.	1060.5	1060.7	267	1012	1058	1056.5-1055.4	1048	1070
$\nu_{11}(a)$	sym. OCO stret.	1029.3	1028.3	95	1003	1027		1019	1024
$\nu_{12}(b)$	ČH rock	1013.3	1010.9	18	1006			1010	985
$\nu_{13}(a)$	OCO bend	544.1	545.4	50	554		547.7-545.4	538	545
$\nu_{14}(a)$	sym. COH torsion	358.6	366.4	64	376			368	366
$\nu_{15}(b)$	anti. COH torsion	325.0	333.0	149	367			333	349

<sup>&</sup>lt;sup>a</sup> Anharmonic intensities given in km mol<sup>-1</sup> calculated at the MP2/aug-cc-pVTZ level. <sup>b</sup> Assignments given here differ from those originally estimated by Lugez et al.

298 K imply that the  $C_s$  form will have no observable contribution to the spectrum generated previously.

Additionally, the calculated frequency of the  $\nu_{10}$  antisymmetric O-C-O stretch at 1060.7 cm<sup>-1</sup>, given in Table 1, lines up almost exactly with the experimental data of Jian et al. at 1058 cm<sup>-1</sup>.<sup>21</sup> This is a significant improvement over the previous B3LYP/aug-cc-pVTZ computations, which place the  $\nu_{10}$ frequency at 1012 cm<sup>-1</sup> before empirical correction. The F12-TZ-cCR QFF VPT2  $\nu_{11}$  symmetric O-C-O stretch at 1028.3 cm<sup>-1</sup> also agrees excellently with the experimental value of 1027 cm<sup>-1</sup>. The purely uncorrected, ab initio F12-TZ-cCR data produced in this work, furthermore, agrees significantly more closely with Jian et al.'s experimental data than does the previous theoretical work given in Table 1 utilized to confirm the gas phase presence of methanediol. The other, previous, scaled harmonic QCISD work of Barrientos et al. 17 places  $\nu_{10}$  at 1070 cm<sup>-1</sup> and  $\nu_{11}$  at 1024 cm<sup>-1</sup>, which are the closest values from previous theory even though they are 10 cm<sup>-1</sup> and 3 cm<sup>-1</sup> away from experiment, respectively.

F12-TZ-cCR also compares well with the Argon matrix data from Lugez et al.<sup>20</sup> The  $\nu_3$  frequency agrees within 1 cm<sup>-1</sup>, as does the  $\nu_8$  frequency. The  $\nu_{10}$ ,  $\nu_{13}$ , and  $\nu_2$  frequencies agree to within 4 cm<sup>-1</sup>. The other fundamental frequencies agree reasonably, with the largest difference being the  $\nu_6$  frequency with a difference of 20.1 cm<sup>-1</sup> from the experimental lower bound. Agreement is generally closer between the Argon matrix data and that from the F12-TZ-cCR QFF than any previous theory, with a couple of exceptions. For the  $\nu_7$  mode, the scaled QCISD data of Barrientos et al. matches 1.1 cm<sup>-1</sup> more closely to the upper bound than F12-TZ-cCR does to the lower bound. Similarly, for the  $\nu_{13}$  mode the QCISD data matches more closely by 0.9 cm<sup>-1</sup>. The QCISD data and Jian et al.'s B3LYP data are approximately 10 cm<sup>-1</sup> closer for the  $\nu_6$  mode, also. However, no other data are as consistently representative as that reported herein implying that this full set of fundamental, anharmonic frequencies are the most accurate produced to date.

Rotational constants from this work and previous theory are given in Table 2. Similar agreement is seen across levels of theory, but the F12-TZ-cCR values are known to be within 7.5 MHz (0.05%) of experiment implying that these computed herein should be exceptionally reliable.43 Additionally, the vibrationally-averaged rotational constants are provided herein for every vibrational mode by the F12-XZ-cCR theories. Distortion constants are also give in Table 3, providing the means to simulate accurate spectra for additional rovibrational features of methanediol.

The  $\nu_{10}$  and  $\nu_{11}$  frequencies have the highest intensities for the  $C_2$  conformation, at 95 and 267 km mol<sup>-1</sup>, thus the previously reported rovibrational feature at 980–1100 cm<sup>-1</sup> will likely be the most significant fingerprint for gas phase methanediol. The  $u_{14}$ and  $\nu_{15}$  frequencies have respectable intensities at 64 and 149 km mol<sup>-1</sup>, respectively, providing an additional means of detecting this molecule in the far infrared/terahertz region.

Table 5 gives anharmonic vibrational frequencies for the  $C_s$ conformation of methanediol. This conformation, although higher in energy, has a significantly higher dipole moment of

Table 2 C2 methanediol rotational constants in MHz

	F12-cCR		Jian et al. <sup>21</sup>	Barrientos et al.17
Parameter	TZ	DZ	B3LYP	CCSD(T)/aVTZ
$A_e$	42038.1	42001.5	41973.9	41669.1
$B_e$	10290.7	10272.4	10118.0	10183.5
$C_e$	9112.2	9097.8	8981.8	9017.7
$A_0$	41613	41566.3	41548.2	
$B_0$	10205.8	10190.5	10043.0	
$C_0$	9018	9004.8	8891.8	
$A_1$	41473.2	41426.8		
$B_1$	10204.7	10189.5		
$C_1$	9015.6	9002.5		
$A_2$	41467.1	41421.7		
$B_2$	10204.8	10189.6		
$C_2$	9015.5	9002.4		
$A_3$	41547.3	41500.3		
$B_3$	10219.7	10204.6		
$C_3$	9026.1	9013		
$A_4$	41500.9	41454.2		
$B_4$	10212.1	10196.9		
$C_4$	9024.7	9011.5		
$A_5$	41520.8	41474.4		
$B_5$	10193.4	10178.1		
$C_5$	9009.4	8996.3		
$A_6$	41566.6	41519.7		
$B_6$	10211.6	10196.1		
$C_6$	9012.5	8999.3		
$A_7$	41645.8	41595.7		
$B_7$	10204.4	10189		
$C_7$	9048.9	9034.8		
$A_8$	41511.7	41464		
$B_8$	10206.7	10191.8		
$C_8$	8982.2	8969.9		
$A_9$	41537	41489.4		
$B_9$	10188.1	10173.4		
$C_9$	9006.5	9003.2	44054.4	
$A_{10}$	41298.8	41254.2	41254.4	
$B_{10}$	10147.6	10132.5	10004.1	
$C_{10}$	8968.2	8955.2	8828.9	
$A_{11}$	41692.5	41657.6	41734.1	
$B_{11}$	10162.5	10147.2	9998.1	
$C_{11}$	8986.7	8973.6	8870.9	
$A_{12}$	41403	41345.3		
$B_{12}$	10176.8	10161.5		
$C_{12}$	8990.2	8967.2		
$A_{13}$	41822.4	41774.6		
$B_{13}$	10174.4	10159.5		
$C_{13}$	8984.4	8971.3		
$A_{14}$	41958.6 10185.7	41908.9 10175.9		
$B_{14}$				
$C_{14}$	9002.8 41399.8	8991.5 41336.9		
$A_{15}$	10224.8	10208.8		
$B_{15}$	9008.4	10208.8 8994.6		
$C_{15}$	9008.4	0994.0		

2.72 D (Table S6, ESI†) compared to the 0.055 D dipole moment of the  $C_2$  conformation, potentially rendering it detectable in the microwave region if present in high enough concentrations. It also has several bright intensity fundamental vibrational frequencies which may give rise to distinct spectral features at high temperatures. The  $\nu_{10}$  and  $\nu_{14}$  frequencies are exceptionally bright, with intensities of 237 km mol<sup>-1</sup> and 112 km mol<sup>-1</sup>, respectively, and the  $\nu_{15}$  frequency has a respectable intensity of 64 km mol<sup>-1</sup>. Looking at F12-TZ-cCR, the  $\nu_{10}$  frequency of the  $C_s$  conformation is shifted by 5.2 cm<sup>-1</sup> from the corresponding frequency of the  $C_2$  conformation,

**Table 3**  $C_2$  methanediol distortion constants

Parameter	Units	F12-TZ-cCR	F12-DZ-cCR		
$\overline{\Delta_I}$	kHz	10.924	10.904		
$\Delta_K$	kHz	417.637	418.185		
	MHz	-0.0516	-0.0517		
$\delta_I$	kHz	2,274	2.272		
$\begin{array}{l} \varDelta_{JK} \\ \delta_{J} \\ \delta_{JK} \\ \Phi_{J} \end{array}$	kHz	23.341	23.353		
$\check{\Phi}_I$	MHz	22.93	23.518		
$\Phi_{K}^{'}$	Hz	15.352	15.307		
$\Phi_{JK}$	MHz	97.769	95.849		
$\Phi_{K\!J}$	Hz	-3.604	-3.599		
$\phi_j$	MHz	10.361	10.651		
$\phi_{jk}$	MHz	147.597	160.424		
$\phi_k$	Hz	6.6	6.85		
$\mu_{\mathbf{y}}$	D	0.06			
μ	D	0.06			

while the  $\nu_{11}$  frequency has a negligible intensity of 26 km mol<sup>-1</sup>. This may result in potential, high-temperature astronomical spectra presenting a less prominent shoulder than seen in the 980–1060 cm<sup>-1</sup> region of Fig. 2 for the  $C_2$  conformation. The  $\nu_{14}$ frequency has a nearly overlapping origin with the  $\nu_{15}$  frequency of the  $C_2$  conformation, at 336.2 cm<sup>-1</sup> compared to 332.5 cm<sup>-1</sup> for F12-TZ-cCR, which may result in an appreciable change of this feature at high temperatures. Frequencies from previous theoretical work are also given in Table 5 for the  $C_s$ conformation. Additionally, rotational constants, distortion constants and geometrical parameters are given in Tables S5 and S6 (ESI†), allowing for modelling of spectra for this conformation.

Comparison between F12-TZ-cCR and F12-DZ-cCR is quite favorable for the latter for both conformations. For the  $C_2$ conformer, the anharmonic vibrational frequencies have a mean absolute difference (MAD) of 4.0 cm $^{-1}$ . The bright  $\nu_{10}$ and  $\nu_{11}$  frequencies have a difference of 0.2 cm<sup>-1</sup> and 1.0 cm<sup>-1</sup>, respectively. Similarly, the rotational constants for F12-DZ-cCR have an MAD of 25.2 MHz relative to F12-TZ-cCR. The geometries for each method, given in Table 4, are nearly identical. Distortion constants, given in Table 3 also compare reasonably, with the possible exception of the  $\phi_{ik}$  constant, with a difference of 12.827 MHz between the two methods.

In comparing F12-TZ-cCR and F12-DZ-cCR for the  $C_s$  conformation, the vibrational frequencies have an MAD of 3.4 cm<sup>-1</sup>. The bright intensity  $\nu_{10}$ ,  $\nu_{11}$ , and  $\nu_{14}$  frequencies differ by 1 cm<sup>-1</sup> or less between the two methods, although the reasonably intense  $\nu_{15}$  frequency is 12.2 cm<sup>-1</sup> higher for F12-DZ-cCR, which

Table 4  $C_2$  methanediol geometry

Parameter	Units	F12-TZ-cCR	F12-DZ-cCR	
r <sub>0</sub> (C1-H2/3)	Å	1.100	1.100	
$r_0(C1-O4/5)$	Å	1.409	1.410	
$r_0(O4-H6)$	Å	0.949	0.949	
$r_0(O5-H7)$	Å	0.949	0.949	
$\angle_{0}(C1-H2-H3)$	deg	109.945	109.932	
$\angle_0$ (C1-O4-H2)	deg	111.775	111.777	
$\angle_{0}(C1-O5-H3)$	deg	111.775	111.777	
$\angle_{0}(O4-C1-H6)$	deg	108.266	108.158	
$\angle_{0}(O5-C1-H7)$	deg	108.266	108.158	

**Table 5**  $C_s$  methanediol anharmonic vibrational frequencies in cm<sup>-1</sup>

		F12-XZ-cCR		Jian et al. <sup>21</sup>	Barrientos et al. <sup>17</sup>		
Mode	Description	TZ	DZ	Int.a	B3LYP	MP2	QCISD
$\overline{\nu_1(a'')}$	anti. OH stret.	3665.3	3668.4	20	3623	3669	3725
$\nu_2(a')$	sym. OH stret.	3662.5	3665.8	47	3622	3667	3724
$\nu_3(a')$	CH <sub>2</sub> stret.	2995.1	2993.3	21	2980	3053	3042
$\nu_4(a')$	CH <sub>1</sub> stret.	2885.1	2890.2	47	2864	2846	2926
$\nu_5(a')$	CH <sub>2</sub> sciss.	1495.3	1499.5	1	1478	1451	1487
$\nu_6(a'')$	CH <sub>2</sub> wag	1408.1	1414.9	20	1404	1416	1405
$\nu_7(a')$	CH <sub>2</sub> twist	1372.2	1370.9	17	1363	1359	1380
$\nu_8(a'')$	COH bend	1344.6	1342.5	1	1320	1336	1343
$\nu_9(a'')$	COH bend	1140.3	1142.8	55	1149	1131	1138
$\nu_{10}(a'')$	anti. OCO stret.	1055.3	1054.3	237	1029	1040	1065
$\nu_{11}(a')$	sym. OCO stret.	1055.4	1052.4	26	1004	1048	1044
$\nu_{12}(a')$	CH <sub>2</sub> rock	997.1	999.2	54	980	995	976
$\nu_{13}(a')$	OCO bend	537.0	535.2	11	526	530	525
$\nu_{14}(a')$	sym. COH torsion	336.2	336.5	112	307	331	363
$\nu_{15}(a'')$	anti. COH torsion	119.6	131.8	64	63	112	155

<sup>&</sup>lt;sup>a</sup> Anharmonic intensities given in km mol<sup>-1</sup> calculated at the MP2/augcc-pVTZ level.

is the largest discrepancy between the two QFFs. The geometries, given in Table S4 (ESI†) are virtually identical. The distortion constants are similar with the exception of the  $\Delta_{IK}$  constant, which is 2.816 kHz for F12-TZ-cCR versus 4.906 kHz for F12-DZcCR. The rotational constants between the two methods have an MAD of 25.5 MHz for the  $C_s$  conformation.

#### 4 Conclusion

Simulated spectra from state-of-the-art, purely ab initio F12-TZcCR OFFs confirm the assignment of the 980-1100 cm<sup>-1</sup> rovibrational feature reported by Chen and Chu<sup>26</sup> as arising from gaseous methanediol. The unadulterated F12-TZ-cCR rovibrational spectrum matches exceptionally well with the experimentally observed spectral features arising from the  $\nu_{10}$  and  $\nu_{11}$ vibrational transitions and agrees with the experimental band origins to within 3 cm<sup>-1</sup>. Additional rovibrational data are also provided in order to produce a complete rovibrational spectral characterization of this molecule in both  $C_2$  and  $C_s$  conformations. Most notably, the  $C_s$  conformation, lying only 781 cm<sup>-1</sup>  $(9.34 \text{ kJ mol}^{-1})$  above the 0.055 D  $C_2$ , has a much larger dipole moment at 2.72 D implying that microwave studies and radioastronomical observations would be more likely to find this higher-energy  $C_s$  conformer than the  $C_2$ . The F12-DZ-cCR approach is additionally shown to achieve excellent accuracy relative to the more costly F12-TZ-cCR, with an MAD of 4.0 cm<sup>-1</sup> relative to the latter for vibrational frequencies and 25.2 MHz for rotational constants for the  $C_2$  conformation. The data provided herein should serve to facilitate possible future astronomical or atmospheric detection of methanediol as well as further classification and examination in the laboratory.

#### Author contributions

Megan C. Davis was responsible for spectral simulations, writing the original draft and supervision. Noah R. Garrett was responsible for investigation via performing theoretical calculations and contributed to the original draft. Ryan C. Fortenwas responsible for conceptualization, administration, and supervision, as well as review and editing for the manuscript.

### Conflicts of interest

There are no conflicts of interest to declare.

### Acknowledgements

Funding is acknowledged from NSF grant NSF-1757220 for support of MCD, NASA grant NNX17AH15G for support of RCF, and start-up funds provided by the University of Mississippi for all three authors. Additionally, the computing resources were provided in part by the Mississippi Center for Supercomputing Research funded with contributions from NSF grant CHE-1757888.

#### Notes and references

- 1 J. L. Axson, K. Takahashi, D. O. D. Haan and V. Vaida, Proc. Natl. Acad. Sci. U. S. A., 2010, 107, 6687-6692.
- 2 M. K. Hazra, J. S. Francisco and A. Sinha, J. Phys. Chem. A, 2014, 118, 4095-4105.
- 3 B. Franco, T. Blumenstock, C. Cho, L. Clarisse, C. Clerbaux, P. F. Coheur, M. D. Mazière, I. D. Smedt, H. P. Dorn, T. Emmerichs, H. Fuchs, G. Gkatzelis, D. W. T. Griffith, S. Gromov, J. W. Hannigan, F. Hase, T. Hohaus, N. Jones, A. Kerkweg, A. Kiendler-Scharr, E. Lutsch, E. Mahieu, A. Novelli, I. Ortega, C. Paton-Walsh, M. Pommier, A. Pozzer, D. Reimer, S. Rosanka, R. Sander, M. Schneider, K. Strong, R. Tillmann, M. V. Roozendael, L. Vereecken, C. Vigouroux, A. Wahner and D. Taraborrelli, Nature, 2021, **593**, 233-237.
- 4 J. de Gouw and D. Farmer, *Nature*, 2021, **593**, 198–199.
- 5 W. L. Chameides and D. D. Davis, Nature, 1983, 304,
- 6 S. Yu, Atmos. Res., 2000, 53, 185-217.
- 7 O. Welz, J. D. Savee, D. L. Osborn, S. S. Vasu, C. J. Percival, D. E. Shallcross and C. A. Taatjes, Science, 2012, 335, 204-207.
- 8 M. I. Lester and S. J. Klippenstein, Acc. Chem. Res., 2018, 51, 978-985.
- 9 R. T. Garrod, S. L. W. Weaver and E. Herbst, Astrophys. J., 2008, 682, 283-302.
- 10 W. A. Schutte, L. J. Allamandola and S. A. Sandford, Icarus, 1993, 104, 118-137.
- 11 F. Duvernay, A. Rimola, P. Theule, G. Danger, T. Sanchez and T. Chiavassa, Phys. Chem. Chem. Phys., 2014, 16, 24200-24208.
- 12 H. Matsuura, M. Yamamoto and H. Murata, Spectrochim. Acta, Part A, 1980, 36, 321-327.

- 13 G. I. M. V. D. O. G. F. Ryabova and R. S. Voloshenko, Russ. J. Appl. Chem., 2002, 75, 22-24.
- 14 K. Z. Gaca-Zajac, B. R. Smith, A. Nordon, A. J. Fletcher, K. Johnston and J. Sefcik, Vib. Spectrosc., 2018, 97, 44-54.
- 15 N. Lebrun, P. Dhamelincourt, C. Focsa, B. Chazallon, J. L. Destombes and D. Prevost, J. Raman Spectrosc., 2003, 34, 459-464.
- 16 G. R. Möhlmann, J. Raman Spectrosc., 1987, 18, 199-203.
- 17 C. Barrientos, P. Redondo, H. Martínez and A. Largo, Astrophys. J., 2014, 784, 132.
- 18 P. Delcroix, M. Pagliai, G. Cardini, D. Bégué and B. Hanoune, J. Phys. Chem. A, 2015, 119, 290-298.
- 19 B. M. Hays and S. L. W. Weaver, J. Phys. Chem. A, 2013, 117, 7142-7148.
- 20 C. Lugez, A. Schriver, R. Levant and L. Schriver-Mazzuoli, Chem. Phys., 1994, 181, 129-146.
- 21 H.-Y. Jian, C.-T. Yang and L.-K. Chu, Phys. Chem. Chem. Phys., 2021, 23, 14699-14705.
- 22 A. D. Becke, J. Chem. Phys., 1993, 98, 5648-5652.
- 23 C. T. Lee, W. T. Yang and R. G. Parr, Phys. Rev. B: Condens. Matter Mater. Phys., 1988, 37, 785-789.
- 24 T. H. Dunning, J. Chem. Phys., 1989, 90, 1007-1023.
- 25 C. Zhu, N. F. Kleimeier, A. M. Turner, S. K. Singh, R. C. Fortenberry and R. I. Kaiser, Proc. Natl. Acad. Sci. U. S. A., 2021, 119, e2111938119.
- 26 Y.-F. Chen and L.-K. Chu, Chem. Commun., 2022, 58, 4208-4210.
- 27 K. Raghavachari, G. W. Trucks, J. A. Pople and M. Head-Gordon, Chem. Phys. Lett., 1989, 157, 479-483.
- 28 I. Shavitt and R. J. Bartlett, Many-Body Methods in Chemistry and Physics: MBPT and Coupled-Cluster Theory, Cambridge University Press, Cambridge, 2009.
- 29 T. D. Crawford and H. F. Schaefer III, in Reviews in Computational Chemistry, ed. K. B. Lipkowitz and D. B. Boyd, Wiley, New York, 2000, vol. 14, pp. 33-136.
- 30 X. Huang, P. R. Taylor and T. J. Lee, J. Phys. Chem. A, 2011, 115, 5005-5016.
- 31 R. C. Fortenberry, X. Huang, J. S. Francisco, T. D. Crawford and T. J. Lee, J. Chem. Phys., 2012, 136, 234309.
- 32 R. C. Fortenberry, X. Huang, J. S. Francisco, T. D. Crawford and T. J. Lee, J. Phys. Chem. A, 2012, 116, 9582-9590.
- 33 D. Zhao, K. D. Doney and H. Linnartz, Astrophys. J., Lett., 2014, 791, L28.
- 34 W. J. Morgan and R. C. Fortenberry, J. Phys. Chem. A, 2015, 119, 7013-7025.
- 35 R. A. Theis and R. C. Fortenberry, Molec. Astrophys., 2016, 2,
- 36 L. Bizzocchi, V. Lattanzi, J. Laas, S. Spezzano, B. M. Giuliano, D. Prudenzano, C. Endres, O. Sipilä and P. Caselli, Astron. Astrophys., 2017, 602, A34.
- 37 M. J. R. Kitchens and R. C. Fortenberry, Chem. Phys., 2016, 472, 119-127.
- 38 R. C. Fortenberry and J. S. Francisco, Astrophys. J., 2017, 835, 243.
- 39 A. Fuente, J. R. Goicoechea, J. Pety, R. L. Gal, R. Martn-Doménech, P. Gratier, V. Guzmán, E. Roueff, J. C. Loison, G. M. M. Caro, V. Wakelam, M. Gerin, P. Riviere-Marichalar and T. Vidal, Astrophys. J., Lett., 2017, 851, 49.

**PCCP** 

- 40 J. P. Wagner, D. C. McDonald II and M. A. Duncan, Angew. Chem., Int. Ed., 2018, 57, 5081-5085.
- 41 R. C. Fortenberry and T. J. Lee, Ann. Rep. Comput. Chem, 2019, 15, 173-202.
- 42 M. B. Gardner, B. R. Westbrook, R. C. Fortenberry and T. J. Lee, Spectrochim. Acta, Part A, 2021, 248, 119184.
- 43 A. G. Watrous, B. R. Westbrook and R. C. Fortenberry, J. Phys. Chem. A, 2021, 125, 10532-10540.
- 44 T. B. Adler, G. Knizia and H.-J. Werner, J. Chem. Phys., 2007, **127**, 221106.
- 45 H. J. Werner, P. J. Knowles, G. Knizia, F. R. Manby, M. Schütz, P. Celani, W. Györffy, D. Kats, T. Korona, R. Lindh, A. Mitrushenkov, G. Rauhut, K. R. Shamasundar, T. B. Adler, R. D. Amos, A. Bernhardsson, A. Berning, D. L. Cooper, M. J. O. Deegan, A. J. Dobbyn, F. Eckert, E. Goll, C. Hampel, A. Hesselmann, G. Hetzer, T. Hrenar, G. Jansen, C. Köppl, Y. Liu, A. W. Lloyd, R. A. Mata, A. J. May, S. J. McNicholas, W. Meyer, M. E. Mura, A. Nicklass, D. P. O'Neill, P. Palmieri, D. Peng, K. Pflüger, R. Pitzer, M. Reiher, T. Shiozaki, H. Stoll, A. J. Stone, R. Tarroni, T. Thorsteinsson and M. Wang, MOL-PRO, Version 2015.1, a Package of Ab Initio Programs, 2015.
- 46 M. Douglas and N. Kroll, Ann. Phys., 1974, 82, 89-155.
- 47 W. D. Allen and coworkers, INTDER2005 is a General Program Written by W. D. Allen and Coworkers, which Performs Vibrational Analysis and Higher-Order Non-Linear Transformations, 2005.
- 48 J. F. Gaw, A. Willets, W. H. Green and N. C. Handy, in Advances in Molecular Vibrations and Collision Dynamics, ed.

- J. M. Bowman and M. A. Ratner, JAI Press, Inc., Greenwich, Connecticut, 1991, pp. 170-185.
- 49 I. M. Mills, in Molecular Spectroscopy Modern Research, ed. K. N. Rao and C. W. Mathews, Academic Press, New York, 1972, pp. 115-140.
- 50 J. K. G. Watson, in Vibrational Spectra and Structure, ed. J. R. During, Elsevier, Amsterdam, 1977, pp. 1–89.
- 51 D. Papousek and M. R. Aliev, Molecular Vibration-Rotation Spectra, Elsevier, Amsterdam, 1982.
- 52 M. J. Frisch, G. W. Trucks, H. B. Schlegel, G. E. Scuseria, M. A. Robb, J. R. Cheeseman, G. Scalmani, V. Barone, G. A. Petersson, H. Nakatsuji, X. Li, M. Caricato, A. V. Marenich, J. Bloino, B. G. Janesko, R. Gomperts, B. Mennucci, H. P. Hratchian, J. V. Ortiz, A. F. Izmaylov, J. L. Sonnenberg, D. Williams-Young, F. Ding, F. Lipparini, F. Egidi, J. Goings, B. Peng, A. Petrone, T. Henderson, D. Ranasinghe, V. G. Zakrzewski, J. Gao, N. Rega, G. Zheng, W. Liang, M. Hada, M. Ehara, K. Toyota, R. Fukuda, J. Hasegawa, M. Ishida, T. Nakajima, Y. Honda, O. Kitao, H. Nakai, T. Vreven, K. Throssell, J. A. Montgomery, Jr., J. E. Peralta, F. Ogliaro, M. J. Bearpark, J. J. Heyd, E. N. Brothers, K. N. Kudin, V. N. Staroverov, T. A. Keith, R. Kobayashi, J. Normand, K. Raghavachari, A. P. Rendell, J. C. Burant, S. S. Iyengar, J. Tomasi, M. Cossi, J. M. Millam, M. Klene, C. Adamo, R. Cammi, J. W. Ochterski, R. L. Martin, K. Morokuma, O. Farkas, J. B. Foresman and D. J. Fox, Gaussian 16 Revision C.01, 2016, Gaussian Inc., Wallingford CT.
- 53 C. M. Western, J. Quant. Spectrosc. Radiat. Transfer, 2017, 186, 221-242.